Article

Thermally Sprayed Aluminum Coatings for the Protection of Subsea Risers and Pipelines Carrying Hot Fluids

Nataly Ce [1,2] and Shiladitya Paul [2,*

[1] School of Engineering, Federal University of Rio Grande do Sul, Porto Alegre 90040-060, Brazil; natalyce@hotmail.com
[2] TWI Ltd, Cambridge, CB21 6AL, UK
* Correspondence: shiladitya.paul@twi.co.uk; Tel.: +44-1223-899-000

Abstract: This paper reports the effect of boiling synthetic seawater on the performance of damaged Thermally Sprayed Aluminum (TSA) on carbon steel. Small defects (4% of the sample's geometric surface area) were drilled, exposing the steel, and the performance of the coating was analyzed for corrosion potential for different exposure times (2 h, 335 h, and 5000 h). The samples were monitored using linear polarization resistance (LPR) in order to obtain their corrosion rate. Scanning electron microscopy (SEM)/energy dispersive X-ray spectroscopy (EDX) and X-ray diffraction (XRD) were used for post-test characterization. The results showed that a protective layer of $Mg(OH)_2$ formed in the damaged area, which protected the underlying steel. Additionally, no coating detachment from the steel near the defect region was observed. The corrosion rate was found to be 0.010–0.015 mm/year after 5000 h in boiling synthetic seawater.

Keywords: thermally sprayed aluminum (TSA); high temperature; corrosion; hot risers

1. Introduction

Coatings are applied on subsea pipelines to protect carbon steel from seawater corrosion, either by acting as a barrier or by providing sacrificial protection. The barrier protection is provided due to the coatings' surface coverage and—in the case of dielectric coatings—a reduction in the corrosion rate results due to the introduction of a high resistance path between anodic and cathodic areas. Coatings for offshore applications must have specific characteristics, such as good adhesion to the steel, resistance to UV degradation, and thermal stability (amongst others), so that they can guarantee corrosion protection in the marine environment [1,2].

Thermally Sprayed Aluminum (TSA) coatings are widely used in offshore industry as a long-term corrosion control method (as sacrificial coatings), suitable for structures subjected to temperatures exceeding 120 °C where a minimum of 200 μm thickness is recommended [2–4]. Sealer is often recommended for TSA to fill surface-connected porosities resulting from the spraying process and prevent the penetration of corrosive substance within the coating. It has been reported that TSA coatings perform better when sealed with organic or silicone sealers; however, one must note that this will increase the cost of the coating process [3–5]. Literature also mentions that inadequate sealing and inappropriate TSA thickness can result in blisters and failure of the coating under certain circumstances [3,6].

Thermal spraying entails propelling small molten or softened particles onto a surface, which when they impact the substrate, flatten and form pancake-shaped splats. The commonly used processes are: electric arc spray, flame spray, plasma spray, high-velocity oxy-fuel spray, detonation gun deposition,

and cold spray [7]. The selection of a process depends on expected coating properties, application, component size, and cost [5].

It is known that dissolved oxygen in water often accelerates corrosion by supporting the cathodic reduction of oxygen. In aluminum corrosion, the air-formed oxide layer on the aluminum surface thickens when exposed to an aqueous environment containing dissolved oxygen. This protective film is stable in the pH range 4–9, and is soluble in strong acids and alkalis. Temperature also affects its behavior, as the corrosion rate of aluminum increases with temperature; however, depending on the exposure environment, a protective film can still be formed, sometimes ultimately decreasing the corrosion rate [8].

During the transportation of oil from a subsea well, the risers and pipelines are subjected to high temperature due to the hot fluid from the reservoir (100–200 °C) [1]. The TSA coating on the outer diameter of a pipeline or riser is therefore expected to be exposed to high temperature seawater, and despite the extensive use of this coating by the offshore industry, not much data is available regarding its performance in high temperature seawater and its protection mechanism, especially when small through-thickness defects (holidays) are present.

This paper presents the performance data of an un-sealed, damaged TSA coating on carbon steel specimens in boiling synthetic seawater. The potential and corrosion rates are also presented, along with the plausible mechanism of calcareous deposit formation on the exposed steel.

2. Materials and Methods

The steel specimens (conforming to BS EN 10027-1 S355J2G4) were TSA coated using a twin-wire arc spray system (TWAS) with a 528 gun. Commercially pure aluminum (99.5 wt.% Al) was used as the spray consumable, and no sealant was applied after spraying. The sample dimensions were Ø 40 mm × 7 mm. Table 1 shows both the steel and Al wire composition, while Table 2 gives the parameters used for the coating production.

Table 1. Composition of the substrate steel and coating (wt.%).

Material	C	Mn	Si	S	P	Fe	N	V	Cu	Al
EN10025S355J2G3	0.12	1.39	0.39	0.019	0.014	Balance	0.003	0.065	–	–
Al wire (coating consumable)	–	<0.01	0.07	–	–	0.21	0.01	–	<0.01	Balance

Table 2. Spray parameters used for the coating production.

Wire Diameter (mm)	Wire Feed Rate (g/min)	Spray Distance (mm)	Increment Step (mm)	Traverse Speed (m/s)	Nominal Thickness (μm)
2.3	98.7	95	15	0.5	200–300

The test consisted of exposing the samples to boiling synthetic seawater for different time periods: 2 h, 335 h, and 5000 h. The ASTM D1141 synthetic seawater composition is given in Table 3, and its pH was 8.2 at 20 °C [9]. Holiday (8 mm defect, 4% of the specimen surface area) was drilled on the coated surface to expose the underlying steel (Figure 1a). The back and edges of samples were covered by a polymeric resin. The specimens were placed in a glass reactor containing the synthetic seawater, and the reactor was heated to bring it to a boil (101 °C). A condenser was used to minimize evaporative water loss. Each specimen was extracted from the test after the specified exposure periods, as stated earlier. The specimen exposed for the longest duration was electrochemically monitored using a potentiostat. A standard three electrode electrochemical setup was used with the TSA-coated specimen (with the holiday) as the working electrode, Pt/Ti as a counter electrode, and a standard calomel electrode (SCE) as a reference connected to the specimen through a polymer salt bridge. The corrosion potential (E_{corr}) was measured, and linear polarization resistance (LPR) technique was used to measure the corrosion rate [10,11].

Table 3. Synthetic seawater composition [9].

Compound	NaCl	MgCl$_2$	Na$_2$SO$_4$	CaCl$_2$	KCl	NaHCO$_3$	KBr	H$_3$BO$_3$	SrCl$_2$	NaF
Concentration (g/L)	24.53	5.20	4.09	1.16	0.695	0.201	0.101	0.027	0.025	0.003

After the experiments, the samples were visually examined and photographed. For metallographic analysis, the samples were sectioned so that analysis of coating cross-sections could be conducted in backscattered electron (BSE) mode under a scanning electron microscope (SEM, Carl Zeiss AG, Oberkochen, Germany). Energy dispersive X-ray spectroscopy (EDX, Carls Zeiss AG, Oberkochen, Germany) was also carried out to have a qualitative chemical analysis of any deposit or corrosion product formed during the exposure. X-ray diffraction (XRD) aiming at the holiday was carried out with Bruker D8 Advance equipment (Bruker Corporation, Billerica, MA, USA) so that the crystalline phases could be identified, complementing the EDX analysis.

3. Results

3.1. Visual Inspection

Photographs of the samples before and after exposure to synthetic seawater can be seen in Figure 1. It can be observed that "whitening" took place on the TSA coating surface, and the holiday area was filled with a white deposit covering the steel surface. No rust was observed on the initially exposed steel surface in the holiday region. No coating damage such as blister or crack was observed.
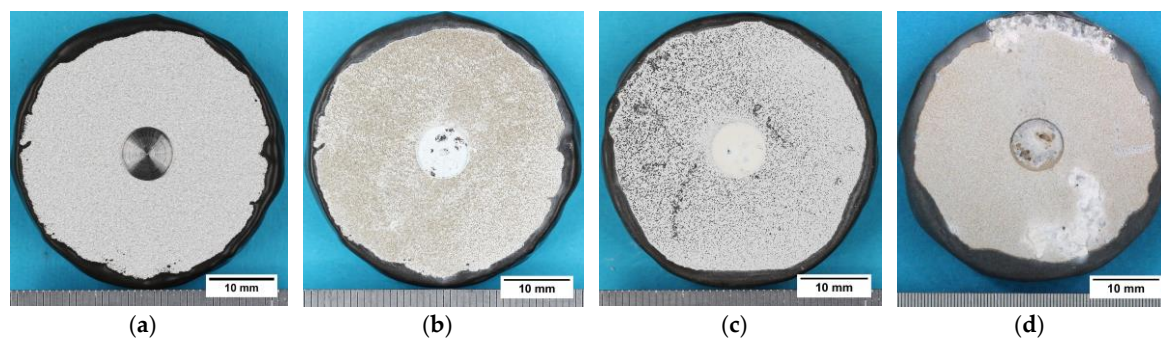

(**a**)　　　　　　　　　(**b**)　　　　　　　　　(**c**)　　　　　　　　　(**d**)

Figure 1. Photographs of samples before (**a**) and after exposure to boiling synthetic seawater for 2 h (**b**), 335 h (**c**) and 5000 h (**d**).

3.2. Corrosion Rate and Potential

3.2.1. Corrosion Rate

Corrosion rate data calculated using LPR technique is shown in Figure 2. Only 10% of the data points are shown for clarity. However, inset shows all data points for the first 40 h of exposure. The extrapolated corrosion rate values calculated at the start of exposure were around 1.3 mm/year. This value dropped to 0.010–0.015 mm/year within the first 200 h of exposure, as can be seen in Figure 2. The drop is most likely due to the formation of deposits on the sample surface—be it on steel or on TSA—thus reducing the galvanic corrosion of TSA. It must be noted that due to the presence of artificially introduced defect (holiday) in the specimen, the data gives the value of corrosion rate for the damaged TSA (taking into account the galvanic effect due to exposed steel) and not the self-corrosion rate of aluminum in seawater. The corrosion rate remained at around 0.010–0.015 mm/year once the initial 200 h period had ended. The discontinuity in the data after 1400 h is due a failure in the data logging system. This, however, did not alter the nature of the plot.
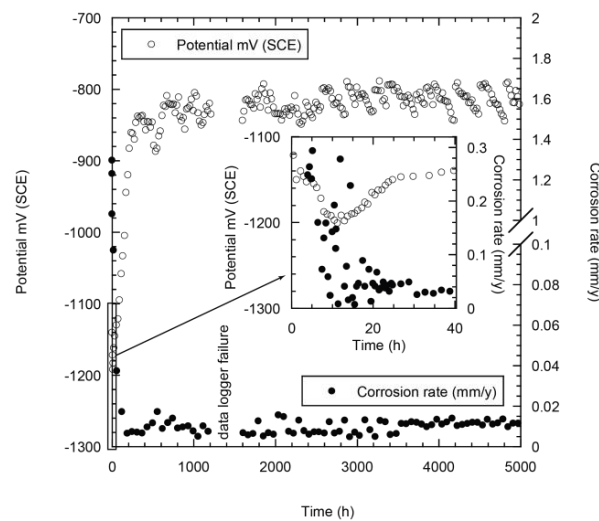
Figure 2. Corrosion rate and potential of a specimen during 5000 h of testing. SCE: standard calomel electrode.

One may argue that LPR corrosion rate measurements of two coupled metals are meaningless. However, due to the small area of steel exposed (4%), the LPR measurements are effectively probing only the galvanic corrosion of the aluminum surface. The data cannot be used as the self-corrosion rate of TSA in boiling seawater, but as the corrosion rate of TSA with a small area (4%) of steel exposed. The galvanic coupling to steel may accelerate the TSA corrosion during the initial exposure period.

3.2.2. Potential (E_{corr})

The open circuit or rest potential of the sample reached a stable value around −800 mV after 600 h of exposure in boiling synthetic seawater (Figure 2). At the beginning of the test, the potential dropped from the initial value of −1120 mV to −1200 mV in the first 10–15 h, after which it started increasing, finally reaching a value of around −800 mV after 5000 h (Figure 2). The initial decrease in potential is probably affected by two things: (i) the dissolution of the air-formed film on TSA in synthetic seawater, and (ii) the reduction in the exposed cathode (steel) due to the formation of a deposit in the holiday region. Formation of an oxide film on TSA coating when in contact with the solution is also likely to play a part.

3.3. Microstructural Characterization

Figure 3 shows the TSA coating layer on the steel surface. This is representative of all samples prior to exposure. The coating comprises some pores, defects, and surface roughness, typical of TSA. The coating thickness was between 200–300 µm.
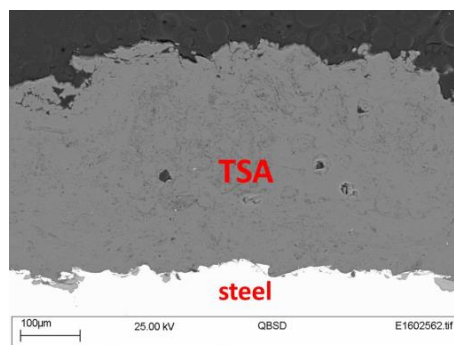

Figure 3. A micrograph showing cross-section of thermally sprayed aluminum (TSA) prior to exposure.

It was easy to detect the deposits in and around the holiday region of the TSA coating by examining coating cross-sections. Figure 4 shows the coating cross-sections under an SEM, and Figures 5 and 6 show the EDX analysis of the marked regions—circle for aluminum oxide film (Al and O), and triangle for Mg-containing film (Mg and O). As the deposits had the same chemical composition, just one result referring to each layer identified is shown, representing all samples.
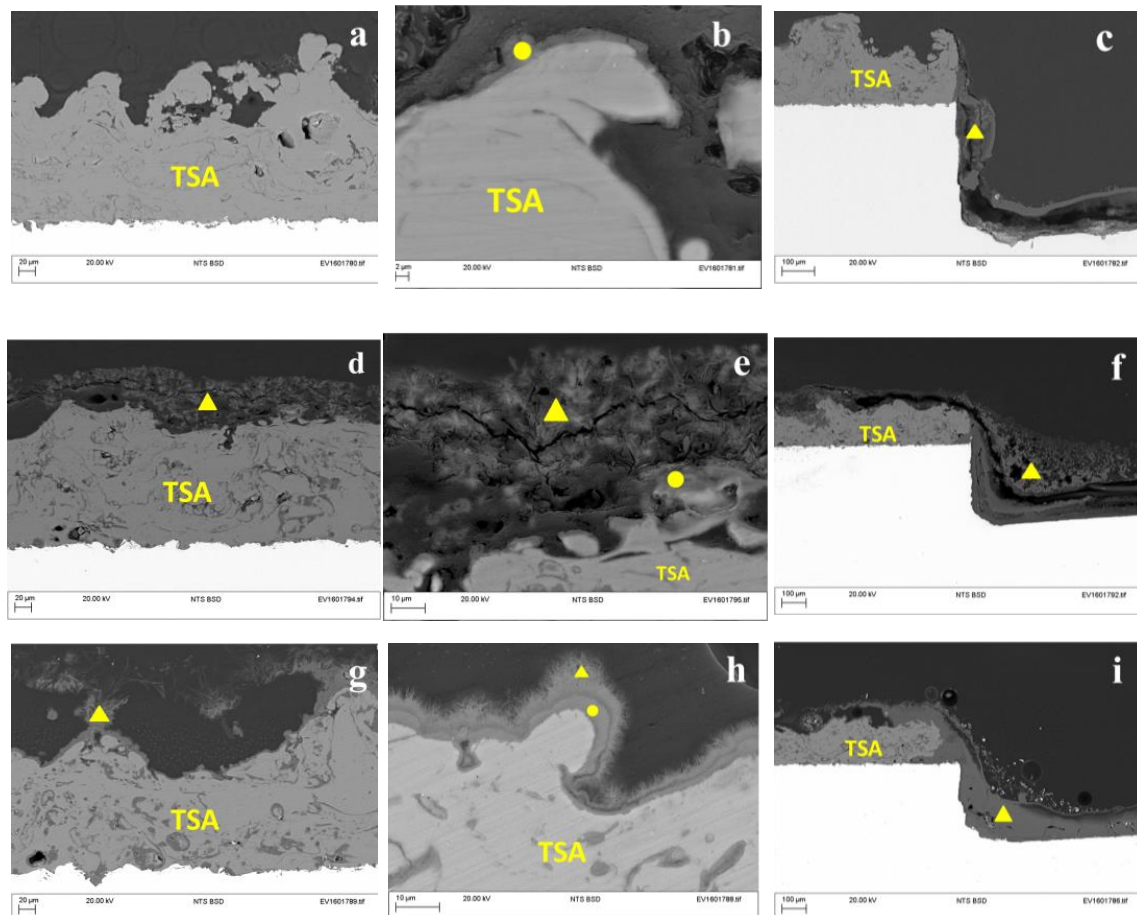

Figure 4. SEM images of specimen cross-sections of TSA and holiday regions showing (**a**) the coating after 2 h exposure; (**b**) top of the TSA coating after 2 h; (**c**) edge of the holiday of 2 h sample; (**d**) TSA coating after 355 h exposure; (**e**) top of the TSA coating in detail after 355 h; (**f**) edge of the holiday after 355 h; (**g**) TSA coating after 5000 h; (**h**) top of the TSA coating in detail after 5000 h; (**i**) edge of the holiday after 5000 h.

Sample exposed for 2 h presented an irregular TSA surface (Figure 4a), and under higher magnification (Figure 4b), a thin film of aluminum oxide was observed. The exposed steel surface was covered by a Mg-containing layer (Figure 4c).

Extended exposure time appears to have been favorable for the growth of Mg-containing compound on TSA coating. Samples exposed for 335 and 5000 h also presented a magnesium layer on the Al-O film apart from the holiday region, as shown in Figure 4d,g respectively; and at higher magnification in Figure 4e,h. Interface TSA–holiday regions can be seen in Figure 4f,i.

The thickness of the TSA coating after exposure of samples was 150 μm. The thickness measured at 10 different locations varied, with the average values being 156 μm, 147 μm, and 154 μm for the specimens tested for 2 h, 335 h, and 5000 h, respectively. The standard deviations for the same specimens were 37 μm, 16 μm, and 32 μm, respectively.
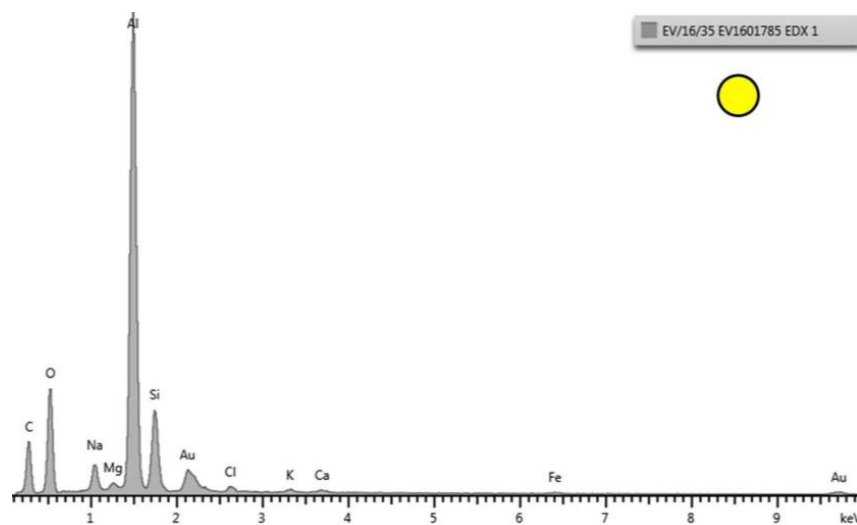
Figure 5. Energy dispersive X-ray spectroscopy (EDX) spectra from the regions marked with a circle in Figure 4. Predominance of Al and O peaks can be observed. This specific pattern is from the sample exposed for 335 h.
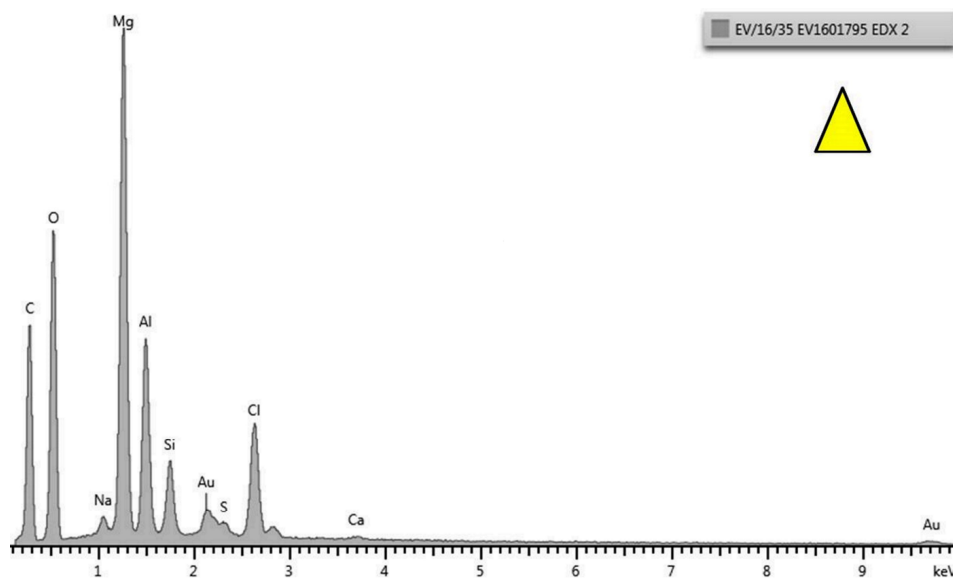

Figure 6. EDX spectra from the regions marked with a triangle in Figure 4. Predominance of Mg and O peaks can be observed. This specific pattern is from the sample exposed for 335 h.

3.4. X-ray Diffraction

The XRD analysis identified the crystalline phases present in the deposit (Figure 7). The analysis was carried out after applying a background correction. The deposit consisted of $Mg(OH)_2$ (brucite), β-Alumina, and mixed hydrated oxides of Mg and Al. Aluminum was present in the pattern due to the presence of TSA in the region next to the holiday. The X-ray beam could not be entirely contained within the holiday, and hence some peaks of Al were observed. Only the (002) β-alumina peak was determined. Some of the other major peaks of β-alumina were masked by the high-intensity peaks of Al, and hence were difficult to determine. Nonetheless, the probability of the presence of β-alumina is realistic.
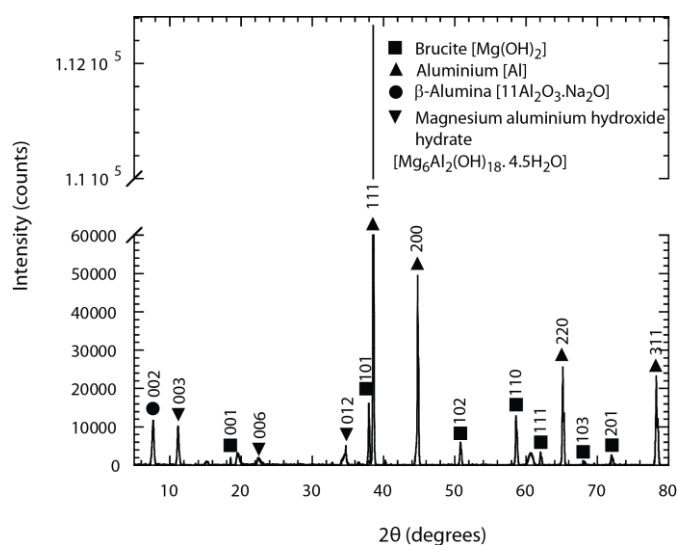
Figure 7. X-ray diffraction (XRD) pattern of the deposit in the holiday region from the specimen exposed for 5000 h.

4. Discussion

It is known that the use of aluminum in marine environments is beneficial, as it generally has good corrosion performance due to the passive surface film formed under normal atmospheric conditions. When breakdown of such film occurs and self-repair is prevented, corrosion will take place [8]. According to the literature, the barrier oxide film comprises two layers: (i) an inner oxide layer, which is a compact amorphous barrier layer strongly bonded to its surface, whose thickness is temperature-dependent; and (ii) an outer layer which is a thicker and more permeable layer of hydrated oxide [8]. Aluminum oxide is stable in the pH range 4 to 9 as mentioned previously; however, the reactions that lead to loss of Al (i.e., its corrosion) depend on the ions present in the solution, their concentration, and the temperature [8,12].

The reduction in potential is initially caused by the breakdown of the air-formed film on TSA coating when in synthetic seawater. In the presence of chlorides, the film repair does not fully occur, allowing corrosion to proceed [13]. The images in Figure 4 show that before all aluminum oxide film was dissolved, a brucite layer was formed on TSA in 355 h and 5000 h samples, preventing further corrosion of the coating. Two hours of exposure appears to be insufficient to allow the growth of brucite on the TSA coating. The reason for the absence of an easily identifiable layer of brucite on TSA in the first few hours of exposure is not entirely clear. However, the kinetic factors governing the nucleation and growth of brucite might have played a role, and hence the layer was only detected after a few hours—probably due to the hydration reaction that happens on aluminum surface prior to calcareous deposit formation [14].

According to the published literature, accelerated corrosion of aluminum occurs between 70 and 80 °C, being less severe beyond these temperatures due to the low dissolved oxygen content in water [12]. No data for the solubility of O_2 in boiling seawater was found; however, a thermodynamic modeling study reported a value of 2.319×10^{-4} (mol/kg) at 89.85 °C and 1 bar pressure in pure water [15]. This is expected to decrease further at 100 °C, and could explain the low corrosion rates in boiling synthetic seawater, where the dissolved oxygen content is likely to be negligible, hence limiting the oxygen diffusion-controlled cathodic reaction on the carbon steel surface [12].

At the start of the test, the potential data represents the mixed potential of aluminum and steel. The presence of holiday ensures a mixed potential behavior, which is a function of the steel and the aluminum surface areas exposed to seawater. As the samples get covered by $Mg(OH)_2$ deposit, the potential decreases (or becomes more negative). The potential curve from Figure 2 and images in Figure 4 suggest that the brucite deposit was present only within the holidays of the samples during the

first 10–15 h of exposure, while the TSA was losing its passive film and slight corrosion was happening in the coating. As the air-formed aluminum oxide film is replaced by the water-formed corrosion product, the potential starts to rise again until it reaches stable values indicative of the protective nature of the deposit formed on both the exposed steel surface and the TSA coating.

Room temperature data suggest that calcareous deposits are usually formed on steel under cathodic protection, being composed of a thin Mg-rich layer on the steel surface with a Ca-rich layer on top of the Mg-rich layer [16–19]. Somehow, the conditions of this experiment did not allow the Ca-rich layer to form. It is also reported that a local pH over 9.5 is required for brucite to form [1,17]. This, however, is only true for lower temperatures, as higher temperatures tend to shift (lower) the neutral point of water as well as the minimum pH required for the precipitation of brucite (Tables 4 and 5).

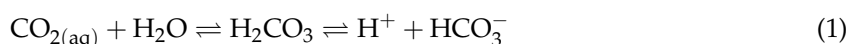**Table 4.** Minimum pH required for the precipitation of $Mg(OH)_2$ in boiling synthetic seawater.

$[OH^-]$ During the Precipitation of Mg $(OH)_2$ in Seawater	Concentration of Mg^{2+} in Synthetic Seawater (mol/L) [9]	K_w at 100 °C (mol²/L²) [25]	pH $= -\log[H^+]$ for Precipitate $Mg(OH)_2$
$[OH^-] = \sqrt{\dfrac{K_{sp}^{Mg(OH)_2}}{[Mg^{2+}]}}$	0.055	6×10^{-13}	6.9

Table 5. Neutral pH calculation of water at 100 °C.

At Neutral Point of Water	Rewriting K_w Expression	$[H^+]$ in mol/L	pH = $-\log[H^+]$
$[OH^-] = [H^+]$	$K_w = [H^+]^2$	7.7×10^{-7}	6.1

The reason for the increase in the surface pH that results in the precipitation of calcareous matter has been studied before [16–20]. The anode (aluminum, in the case of TSA-coated steel) polarizes the steel, resulting in the production of hydroxyl ions (OH^-), which increases the interfacial pH. The generation of OH^- ions occurs either due to the reduction of dissolved oxygen or the reduction of water (which occurs at slightly greater negative potentials).

The carbonates in water follow the relationship through the equilibria in Equations (1) and (2) [21], and so the presence of gases such as CO_2 directly affects the solubility of species in seawater.

$$CO_{2(aq)} + H_2O \rightleftharpoons H_2CO_3 \rightleftharpoons H^+ + HCO_3^- \tag{1}$$

$$HCO_3^- \rightleftharpoons H^+ + CO_3^{2-} \tag{2}$$

Henry's law assumes that the higher the partial pressure (p) of a gas over a liquid, the greater its solubility, and the higher the temperature, the lower its solubility in water [21,22]. The solubility of $CaCO_3$ is dependent on the partial pressure of CO_2 and solution temperature. No experimental data is available for CO_2 solubility at 100 °C; however, a modeling study reported that at a pressure of 0.06 MPa (0.6 bar), the solubility of CO_2 at 80 °C is only 0.003 mol% [23]. Thus, in this current study under boiling seawater temperature and atmospheric pressure, the deposition of $CaCO_3$ is highly unlikely due to the negligible dissolved CO_2 content. Moreover, it should be highlighted that the concentration of Ca^{2+} ions in seawater is only 0.04%, compared to the 0.13% for Mg^{2+} ions.

In the current study, the lack of CO_2 solubility means that the solubility product (K_{sp}) of $Mg(OH)_2$ becomes more relevant, and can explain part of the mechanism related to the formation of the deposit. K_{sp} is the equilibrium constant expressed by the product of the ion concentrations present in a saturated solution representing the solubility of slightly soluble salts [24].

For $Mg(OH)_2$, the dissociation equilibria involved is shown in Equation (3).

$$Mg\,(OH)_2 \overset{aq}{\leftrightarrow} Mg^{2+} + 2OH^- \tag{3}$$

the K_{sp} is given by Equation (4)

$$K_{sp}^{Mg(OH)_2} = [Mg^{2+}][OH^-]^2 \tag{4}$$

The solubility of $Mg(OH)_2$ at 100 °C is 6.9×10^{-5} mol/L [24], so the $K_{sp}^{Mg(OH)_2}$ was calculated to be 1.31×10^{-12} mol^3/L^3 at 100 °C.

Rearranging the ionic product of water (K_w) and pH expression shown in Equations (5) and (6), the values in Table 4 can be calculated.

$$K_w = [OH^-][H^+] \tag{5}$$

$$pH = -\log[H^+] \tag{6}$$

The bulk pH measured at the end of the experiment was 6.3 at room temperature. It must be considered that the neutral pH of water (accepted to be pH 7) is only true at 25 °C. At 100 °C, the neutral point can be calculated following the steps in Table 5, and it was found to be pH 6.1.

The deposition of $Mg(OH)_2$ in boiling temperatures will cease when the local pH is lower than 6.9, as the ionic product of Mg^{2+} and OH^- does not exceed its solubility product at pH < 6.9. The solubility product of brucite, $K_{sp}^{Mg(OH)_2}$, was calculated to be 1.31×10^{-12} mol^3/L^3 at 100 °C. The increase in the concentration of H^+ ions (lower pH) increases the solubility of brucite, due to the shift of Equation (3) to the right, where more $Mg(OH)_2$ will dissolve. Figure 8 shows the mechanism of precipitation based on this study.
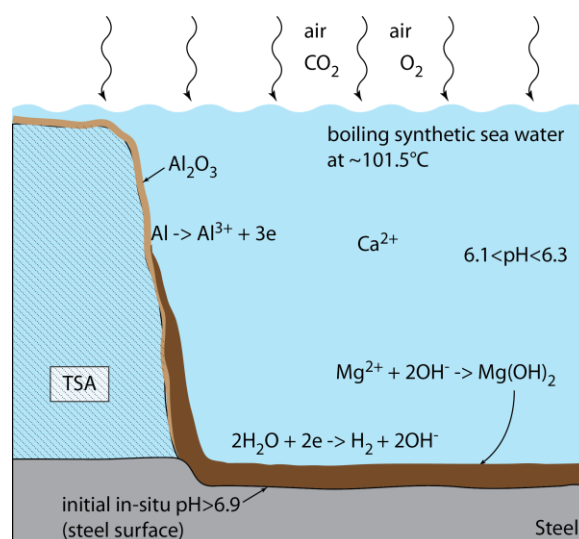

Figure 8. Mechanism of brucite formation on the exposed steel surface in the holiday region.

In summary, the cathodic polarization of exposed steel surface by TSA leads to the generation of OH^- ions. This increase in the steel surface pH results in the deposition of $Mg(OH)_2$, which covers the exposed steel. No deposition of $CaCO_3$ was seen due to the insufficient amount of dissolved CO_2 present in boiling synthetic seawater to shift the calco-carbonic equilibria. However, it must be noted that in natural seawater, the presence of microorganisms may change the calco-carbonic equilibria and the corrosion mechanism.

5. Conclusions

The damaged TSA-coated samples presented low corrosion rate after 5000 h of exposure in boiling synthetic seawater. The stable potential—not too dissimilar for aluminum—after few hours of testing suggests that the samples were protected from the corrosive environment. The coating did not show cracks or damage, and no detachment was observed near the holiday. A brucite layer was deposited on steel and aluminum surface. The brucite layer prevented the consumption of the aluminum coating and the corrosion of the exposed steel area due to its protective properties. A dense layer grew on top

of a porous layer, impeding the diffusion of oxygen towards the sample surface. While the neutral pH of the synthetic seawater was calculated to be around 6.1, the local pH at the sample surface was higher, calculated to be 6.9, allowing the precipitation of $Mg(OH)_2$. A $CaCO_3$ deposit was not observed in boiling seawater, probably influenced by the negligible amount of dissolved CO_2, altering the calco-carbonic equilibrium. In general, one can conclude that a TSA coating could protect steel, even in boiling synthetic seawater when small defects exposing the steel are present.

Author Contributions: Shiladitya Paul conceived, designed and carried out the exposure tests; Nataly Ce carried out the microstructural characterization and wrote the paper; Shiladitya Paul analyzed the data, reviewed the paper and made final changes.

Conflicts of Interest: The authors declare no conflict of interest.

References

1. Palmer, A.C.; Roger, A.K. *Subsea Pipeline Engineering*, 2nd ed.; PennWell: Tulsa, OK, USA, 2008; pp. 247–264.
2. Paul, S. Corrosion Control for Marine- and Land-Based Infrastructure Applications. In *ASM Handbook—Thermal Spray Technology*, 2nd ed.; Robert, C.T., Jr., Ed.; ASM International: Materials Park, OH, USA; Volume 5A, 2013; pp. 248–252.
3. Heidersbach, R. *Metallurgy and Corrosion Control in Oil and Gas Production*, 1st ed.; John Willey & Sons: Hoboken, NJ, USA, 2011.
4. NORSOK M-501. In *Surface Preparation and Protective Coating*; Standards Norway: Oslo, Norway, February 2012.
5. Fauchais, P.; Vardelle, A. Thermal Sprayed Coatings Used Against Corrosion and Corrosive Wear. In *Advanced Plasma Spray Applications*, 1st ed.; Intech: Rijeka, Croatia, 2012; pp. 1–38.
6. Thomason, W.H.; Olsen, S.; Haugen, T.; Fischer, K. Deterioration of Thermal Sprayed Aluminum Coatings on Hot Risers Due to Thermal Cycling. In Proceedings of Corrosion 2004, New Orleans, LA, USA, 28 March–1 April 2004; Paper No. 04021. pp. 1–16.
7. Crawner, D.E. Thermal Spray Processes. In *ASM Handbook—Thermal Spray Technology*; ASM International: Materials Park, OH, USA, 2013; Volume 5A, pp. 54–59.
8. Davis, J.R. Corrosion of Aluminum and Aluminum Alloys. In *ASM Handbook*, 1st ed.; ASM International: Materials Park, OH, USA, 1999; pp. 25–42.
9. *ASTM D1141 Standard Practice for the Preparation of Substitute Ocean Water*; ASTM International: Materials Park, OH, USA, 2013.
10. Stern, M.; Geary, A.L. Electrochemical Polarization: A Theoretical Analysis of the Shape of Polarization Curves. *J. Electrochem. Soc.* **1957**, *104*, 56–63. [CrossRef]
11. Stern, M. A Method for Determining Corrosion Rates from Linear Polarization Data. *Corrosion* **1958**, *14*, 440–444. [CrossRef]
12. Ghali, E.; Revie, R.W. *Corrosion Resistance of Aluminum and Magnesium Alloys: Understanding, Performance, and Testing*, 1st ed.; John Willey & Sons: Hoboken, NJ, USA, 2010; pp. 160–173.
13. Lorking, K.F.; Mayne, J.E.O. The Corrosion of Aluminium. *J. Appl. Chem.* **1961**, *11*, 170–180. [CrossRef]
14. Lajevardi, S.A.; Tafreshi, H.; Shahrabi, T. Investigation of Calcareous Deposits Formation on 5052 Aluminium Alloy under Cathodic Polarisation in Natural and Artificial Sea Water. *Corros. Eng. Sci. Technol.* **2011**, *46*, 249–255. [CrossRef]
15. Geng, M.; Duan, Z. Prediction of Oxygen Solubility in Pure Water and Brines up to High Temperatures and Pressures. *Geochim. Cosmochim. Acta* **2010**, *74*, 5631–5640. [CrossRef]
16. Deslouis, C.; Festy, D.; Gil, O.; Rius, G.; Touzain, S; Tribollet, B. Characterization of Calcareous Deposits in Artificial Seawater by Impedance Techniques—I. Deposit of $CaCO_3$ without $Mg(OH)_2$. *Electrochim. Acta* **1997**, *43*, 1891–1901. [CrossRef]
17. Neville, A.; Morizot, A.P. Calcareous Scales Formed by Cathodic Protection—An Assessment of Characteristics and Kinectics. *J. Crystal Growth* **2002**, *243*, 490–502. [CrossRef]

18. Barchiche, C.; Deslouis, C.; Festy, D.; Gil, O; Refait, P.; Touzain, S.; Tribollet, B. Characterization of Calcareous Deposits in Artificial Seawater by Impedance Techniques 3-Deposit of CaCO$_3$ in the Presence of Mg(II). *Eletrochimica Acta* **2003**, *48*, 1645–1654. [CrossRef]

19. Barchiche, C.; Deslouis, C.; Gil, O.; Joiret, S.; Refait, P.; Tribollet, B. Role of Sulphate Ions on the Formation of Calcareous Deposits on Steel in Artificial Seawater; the Formation of Green Rust Compounds during Cathodic Protection. *Electrochimica Acta* **2009**, *54*, 3580–3588. [CrossRef]

20. Salgavo, G.; Maffi, S.; Magagnin, L.; Benedetti, A.; Pasqualin, S.; Olzi, E. Calcareous Deposits, Hydrogen Evolution and pH on Structures under Cathodic Polarization in Seawater. In Proceedings of the Thirteenth International Offshore and Polar Engineering Conference, Honolulu, HI, USA, 25–30 May 2003.

21. Millero, F.J. Thermodynamics of the Carbon Dioxide System in the Oceans. *Geochim. Cosmochim. Acta* **1995**, *59*, 661–667. [CrossRef]

22. Zeebe, R.E.; Wolf-Gladrow, D. *CO$_2$ in Seawater: Equilibrium, Kinetics, Isotopes*, 1st ed.; Elsevier: Amsterdam, The Netherlands, 2001; pp. 1–3, 63–67, 256.

23. Carrol, J.J.; Slupsky, J.D.; Mather, A.E. The Solubility of Carbon Dioxide in Water at Low Pressure. *J. Phys. Chem.* **1991**, *20*, 1201–1209. [CrossRef]

24. David, R.L. *CRC Handbook of Chemistry and Physics*, 85th ed.; CRC Press: Boca Raton, FL, USA, 2005.

25. Burgot, J.L. *Ionic Equilibria in Analytical Chemistry*, 1st ed.; Springer: New York, NY, USA, 2012.